

Article

Low-Carbon Optimal Scheduling Model for Peak Shaving Resources in Multi-Energy Power Systems Considering Large-Scale Access for Electric Vehicles

Kang Dai ^{1,2}, Kun Zhang ^{1,*}, Jicheng Li ², Liang Liu ², Zhe Chen ^{1,3} and Peng Sun ¹¹ Shenyang University of Technology, Shenyang 110870, China² Northeast Branch of State Grid Corporation of China, Shenyang 110000, China³ Department of Energy Technology, Aalborg University, 9220 Aalborg, Denmark

* Correspondence: zhangkun@sut.edu.cn

Abstract: Aiming at the synergy between a system's carbon emission reduction demand and the economy of peak shaving operation in the process of optimizing the flexible resource peaking unit portfolio of a multi-energy power system containing large-scale electric vehicles, this paper proposes a low-carbon optimal scheduling model for peak shaving resources in multi-energy power systems considering large-scale access for electric vehicles. Firstly, the charging and discharging characteristics of electric vehicles were studied, and a comprehensive cost model for electric vehicles, heat storage, and hydrogen storage was established. At the same time, the carbon emission characteristics of multi-energy power systems and their emission cost models under specific carbon trading mechanisms were established. Secondly, the change characteristics of the system's carbon emissions were studied, and a carbon emission cost model of multi-energy power was established considering the carbon emission reduction demand of the system. Then, taking the carbon emission of the system and the peak regulating operation costs of traditional units, energy storage, and new energy unit as optimization objectives, the multi-energy power system peak regulation multi-objective optimization scheduling model was established, and NSGA-II was used to solve the scheduling model. Finally, based on a regional power grid data in Northeast China, the improved IEEE 30 node multi-energy power system peak shaving simulation model was built, and the simulation analysis verified the feasibility of the optimal scheduling model proposed in this paper.

Keywords: multi-energy storage; peak regulating resources; electric vehicle; carbon reduction



Citation: Dai, K.; Zhang, K.; Li, J.; Liu, L.; Chen, Z.; Sun, P. Low-Carbon Optimal Scheduling Model for Peak Shaving Resources in Multi-Energy Power Systems Considering Large-Scale Access for Electric Vehicles. *Processes* **2023**, *11*, 1532. <https://doi.org/10.3390/pr11051532>

Academic Editors: Qiuye Sun, Rui Wang and Zhengmao Li

Received: 10 April 2023

Revised: 5 May 2023

Accepted: 15 May 2023

Published: 17 May 2023



Copyright: © 2023 by the authors. Licensee MDPI, Basel, Switzerland. This article is an open access article distributed under the terms and conditions of the Creative Commons Attribution (CC BY) license (<https://creativecommons.org/licenses/by/4.0/>).

1. Introduction

In recent years, with gradual improvements in the requirements of environmental protection, governance, and restoration, it has become the focus to explore and develop the new power system structure and power supply system with green, low-carbon and efficient new energy as the main body to achieve carbon peak and carbon neutralization [1,2]. The multi-energy power system is a multi-energy power generation unit with thermal power, hydroelectric power, wind power, photovoltaic, etc., as the energy supply unit, which undertakes the task of multi-energy supply, transmission, conversion, storage, and consumption of the system [3,4]. However, the uncertainty of new energy power sources and multi-energy loads in the multi-energy power system still led to the power and energy regulation and peak adjustment demands on different time and space scales in the actual operation of the system [5,6]. Therefore, it is necessary to study the low-carbon and economic scheduling methods of flexible resources in the multi-energy power system, taking into account the needs of system supply and demand balance, carbon emission reduction, and energy supply economy [7,8].

For the flexible peaking resources in the power system, domestic and foreign scholars have conducted some relevant studies. In references [9,10], aiming at the problem of the

influence of random and uncertain output of new energy power sources in the power grid on the allocation of flexible peak regulation resources, the capacity change regulation compensation of power sources in the power grid was analyzed and studied. Then, a corresponding capacity compensation strategy was designed, and an optimization model of peak regulation income of power sources in the power grid was established to realize the optimization of power grid peak regulation resources under the market mechanism. In references [11–13], the regulation characteristics of nuclear power units, hydropower units, photovoltaic power sources, electric vehicles, etc., in the power grid were analyzed and studied, respectively, and the optimal scheduling model of power grid peak regulation, including the above-mentioned units, was established to improve the power grid peak regulation capacity. In references [14–17], aiming at the power system with large-scale renewable energy access, the influence of the random output of renewable energy on the operation of peak regulating resources in the system under different time scales was analyzed, and a multi-time-scale optimization model of peak regulating resources in the power system considering flexibility was established to improve the system peak regulating ability and flexibility.

For the low-carbon and economic dispatch of peaking units in multi-energy power systems, it is necessary to formulate and solve the low-carbon and economic regulation plan of multi-energy flexible peaking units on the day-ahead or intra-day time scale, on the network-wide or local area spatial scale, so as to optimize the distribution of multi-energy peaking demand in the system among the flexible peaking units, under the premise of ensuring the safe and high-quality operation of the system and based on various equation constraints and inequality constraints, such as the operating characteristics of the flexible resource regulation units of various energy forms involved in peaking in the system [18,19].

In reference [20], it is proposed that while expanding the scale of wind power, low-carbon transformation should be carried out on existing thermal power units, and the adjustable resources of source and load should be fully utilized to improve the wind power absorption capacity of the system, so as to promote the low-carbon power system. In references [21–23], a scheduling strategy for solar thermal power station and wind power system based on a carbon trading mechanism was proposed by combining low-carbon technology with a market mechanism. Through simulation, the proposed strategy can effectively improve the system wind power consumption rate and reduce the system carbon emissions. In reference [24], taking the power system including carbon capture technology as the research object, a two-stage optimization model with the lowest comprehensive cost as the objective function was established to verify the rationality of low-carbon and economic scheduling of peak regulating units in the power system.

V2G (vehicle to grid) technology can achieve the interaction between electric vehicles and the power grid [25]. In reference [26], considering the uncertainty of electric vehicles in the microgrid environment, planning research was conducted with the goal of minimizing the cost of the microgrid system. Some studies also explore the responsiveness and economy of electric vehicle users participating in V2G from the user side. Reference [27] proposed an optimized and orderly charging control strategy for peak and valley time of use pricing considering the responsiveness of electric vehicle users to improve user satisfaction and system operation safety. Reference [28] predicted the daily charging load of large-scale electric vehicles in the long term and analyzed the impact of their access to the distribution network. Reference [29] proposed an interesting concept regarding vehicle-to-vehicle energy interaction devices, which may have spawned a new field. References [30,31] analyzed the elastic distributed frequency estimation method of electric vehicle load frequency regulation based on an intrusion detector under network attack and proposed a distributed economic model predictive control method, which can effectively improve the frequency control ability.

Aiming at the multi-objective optimization and its solution of peak load regulation and low-carbon economic dispatch of multi-energy power systems with large-scale electric vehicles, this paper establishes a low-carbon optimal dispatch model of peak load regulation

resources of a multi-energy power system considering large-scale access for electric vehicles. The innovative contributions of this paper are as follows:

- (1) The charging and discharging characteristics of electric vehicles are analyzed, and the total investment cost of electric vehicles, the performance degradation cost, maintenance cost, and battery energy storage efficiency cost model of the battery charging and discharging cycle are established. Considering the conversion of electrothermal energy storage and electric hydrogen energy storage and their participation in power grid regulation characteristics, the total investment cost, maintenance cost, and operation cost models of electrothermal energy storage and electric hydrogen energy storage are established.
- (2) The carbon emission characteristics of coal-fired units and the carbon emission cost model are studied. The relationship between the actual carbon emissions and the carbon emission quota of the multi-energy power system is analyzed, and a carbon emission cost model of the multi-energy power system is established.
- (3) Considering the nonlinear relationship between multi-energy power system peaking unit commitment and carbon emissions, peaking economy, energy supply reliability, energy supply economy, and safety and stability, a multi-objective optimal scheduling model of a multi-energy power system considering large-scale access of electric vehicles is established. A multi-objective optimization model of a multi-energy power system based on a non-dominated sorting genetic algorithm (NSGA-II) is proposed.

2. Electric Vehicle and Its Comprehensive Cost Model

2.1. Electric Vehicle Model

The optimal scheduling model established in this paper mainly considers the use of V2G to participate in peak shaving on the basis of a certain scale of electric vehicles. In the case of joint output of power supply and electric vehicles, it meets the load demand, stabilizes the load curve, and improves the operation stability [32,33]. The orderly interaction between electric vehicles and power grids through V2G can offset the uncertainty of the output of wind and solar units to a certain extent, improve the consumption of wind and solar output, reduce the output of thermal power units, and achieve carbon reduction [34,35].

The electric vehicle model is as follows:

$$\begin{aligned} P_{EV\min} &\leq P_{CH,t} - P_{DIS,t} \leq P_{EV\max} \\ P_{EV\min} &= -\rho_t E_V p_{DIS} / \eta_{DIS} \\ P_{EV\max} &= \rho_t E_V p_{CH} \eta_{CH} \end{aligned} \quad (1)$$

Since electric vehicles can only be charged or discharged at the same time, the sum of the number of electric vehicles charged or discharged at the same time cannot exceed the total number of electric vehicles.

$$\left\lfloor \frac{P_{CH,t} \eta_{CH}}{p_{CH}} \right\rfloor + \left\lfloor \frac{P_{DIS,t}}{\eta_{DIS} p_{DIS}} \right\rfloor \leq E_V \quad (2)$$

where $(P_{CH,t} \eta_{CH} / p_{CH})$ and $P_{DIS,t} / \eta_{DIS} p_{DIS}$, respectively, represent the number of vehicles charged and discharged, so it is necessary to round them down, which means taking the maximum integer value not greater than the calculated result. $\lfloor \cdot \rfloor$ represents a rounding function.

2.2. Comprehensive Cost Model of Electric Vehicle

For a large-capacity electric vehicle, its comprehensive cost can be considered from four aspects: total system investment cost, performance degradation cost of battery charging and discharging cycle, maintenance cost, and battery energy storage efficiency cost. The specific calculation process is as follows:

2.2.1. Calculation of Total Investment Cost of Electric Vehicle

The total investment cost of the electric vehicle can be described as a quadratic function between the total investment cost and the charging and discharging power, the storage capacity of the electric vehicle, specifically:

$$C_{CBTN,1} = \alpha_{CB0} + \alpha_{CB1}P_{BSIN} + \alpha_{CB2}P_{BSIN}^2 + \beta_{CB1}W_{BSIN} + \beta_{CB2}W_{BSIN}^2 \quad (3)$$

2.2.2. Performance Degradation Cost Calculation of Battery Charge–Discharge Cycle of Electric Vehicle

The performance aging of electric vehicles is mainly due to the attenuation of ion exchange capacity, which is mainly related to the number of battery charging and discharging cycles in the electric vehicle. In addition to the number of cycles, the difference between the charge and discharge power and the rated power is the main factor affecting the capacity attenuation of electric vehicles. Therefore, the capacity attenuation characteristics of chemical batteries in the electric vehicle can be described as:

$$Y_{kcdc} = \lambda_B e^{-k_{CDC}^{\xi} \left(\frac{W_{ACE}}{R_{SEI} T_{emp}} - \phi_{CDC} \right)} \quad (4)$$

$$\phi_{CDC} = \varphi(k_{CDC})(P_{INP} - P_{BSIN}) \quad (5)$$

The change in battery capacity in the electric vehicle is taken as the main indicator of battery aging in the electric vehicle. Then, the battery performance state of the electric vehicle can be expressed as:

$$SOH_{CB} = \frac{W_{NOM} - Y_{kcdc}}{W_{NOM}} = 1 - \frac{Y_{kcdc}}{W_{NOM}} \quad (6)$$

It is assumed that the relationship between the unit capacity of the battery and its corresponding acquisition cost in the electric vehicle is a quadratic function. Then, the performance degradation cost corresponding to a single charge–discharge cycle of the electric vehicle can be further obtained as follows:

$$C_{CBTN,2} = \vartheta_{BSP1}(1 - SOH_{CB})W_{BSIN} + \vartheta_{BSP2}(1 - SOH_{CB})^2W_{BSIN}^2 \quad (7)$$

2.2.3. Maintenance Cost Calculation of Electric Vehicle

After the electric vehicle is put into operation, the necessary maintenance will generate certain expenses, which can be considered as proportional to the total investment cost of the electric vehicle. The maintenance cost of the electric vehicle can be expressed as:

$$C_{CBTN,3} = C_{CBTN,1}R_{CBm} \quad (8)$$

2.2.4. Cost Calculation of Battery Energy Storage Efficiency of Electric Vehicle

During the process of transforming electric energy into chemical energy, a part of electric energy will be lost due to the electrochemical characteristics and thermal effect characteristics of the battery. At the same time, when the electric vehicle releases energy, it is also impossible to fully convert the chemical energy stored in the battery into electric energy due to the chemical and thermal characteristics. In the charge–discharge cycle of the electric vehicle, the ratio of the energy lost in this “electric energy—chemical energy—electric energy” conversion cycle to the electric energy absorbed by the battery is the energy loss rate of the electric vehicle, which can be expressed as:

$$\mu_{BSIN} = \frac{W_{INP} - W_{OUP}}{W_{INP}} \quad (9)$$

In Equation (9), the energy loss corresponding to the battery charging and discharging process of the electric vehicle is converted into electric quantity, and the corresponding electricity price cost is the battery energy storage efficiency cost of the electric vehicle.

Similar to the electric heating energy storage system, if the electric energy stored by the electric vehicle comes from wind power abandonment, the cost brought by energy storage efficiency can be expressed as:

$$C_{CBTN4} = \mu_{BSIN} p_w^t \sum_{t=1}^T P_{wCB}^t \Delta T \quad (10)$$

When the electric vehicle stores electric energy under the condition of non-wind abandonment due to its own operation-mode adjustment, the required electricity cost is generally higher than the cost when purchasing wind abandonment power. In this case, the corresponding energy storage efficiency cost can be expressed as:

$$C_{CBTN5} = \mu_{BSIN} p_g^t \sum_{t=1}^T P_{wCB}^t \Delta T \quad (11)$$

3. Comprehensive Cost Model of Multi-Energy Storage System

3.1. Comprehensive Cost Model of Electric Heating Energy Storage System

For a large-capacity electric heating energy storage system, its comprehensive cost generally includes the total system investment cost, maintenance cost, power purchase cost, and heat purchase cost. The specific calculation process is as follows.

3.1.1. Calculation of Total Investment Cost of Electric Heating Storage System

The total investment cost of electric heating storage system is as follows:

$$C_{EH,1} = C_{he} + C_{hs} + C_{ts} + C_{il} + C_{hv} + C_{el} + C_{gr} + C_{cn} \quad (12)$$

$$\left\{ \begin{array}{l} C_{he} = a_0 + a_1 \overline{P_{ein}} + a_2 \overline{P_{ein}}^2 \\ C_{hs} = b_0 + b_1 \overline{C_{ph}} + b_2 \overline{C_{ph}}^2 \\ C_{ts} = c_0 + c_1 \overline{P_{hout}} + c_2 \overline{P_{hout}}^2 \\ \left\{ \begin{array}{l} C_{il} = p_{ps} S_{ps} \\ V_{ps} = k_{ps} \overline{C_{ph}} / c_{sh} / \rho_{ph} \\ S_{ps} = 2h_{ph} w_{ph} + 2V_{ps} / h_{ph} + 2V_{ps} / w_{ph} \end{array} \right. \\ C_{hv} = d_0 + d_1 \overline{P_{ein}} \\ C_{el} = e_0 \overline{P_{ein}} + e_1 \overline{C_{ph}} + e_2 \overline{P_{hout}} \\ C_{gr} = g_0 \overline{P_{ein}} + g_1 \overline{C_{ph}} + g_2 \overline{P_{hout}} \\ C_{cn} = h_0 \overline{P_{ein}} + h_1 \overline{C_{ph}} + h_2 \overline{P_{hout}} \end{array} \right. \quad (13)$$

In the calculation of the actual operation cost, the total investment cost of the electric heating energy storage system can be simplified. Ignoring the relatively small cost C_{ts} of the gas–water heat exchanger and some other equipment costs, Equation (12) is further fitted and described as a function of the system electric heating power $\overline{P_{ein}}$ and heat storage capacity $\overline{C_{ph}}$, as follows:

$$C_{EH,1} = a_{00} + a_{11} \overline{C_{ph}} + a_{22} \overline{C_{ph}}^2 + b_{11} \overline{P_{ein}} + b_{22} \overline{P_{ein}}^2 \quad (14)$$

3.1.2. Maintenance Cost Calculation of Electric Heating Energy Storage System

When the electric heating energy storage system is running, it needs to carry out necessary maintenance of the system, which will generate certain costs, which can be

considered as proportional to the total investment cost of the system. Therefore, the maintenance cost of the electric heating energy storage system can be expressed as:

$$C_{EH,2} = C_{EH,1} \cdot R_m \quad (15)$$

3.1.3. Cost Calculation of Electric Heating Energy Storage System

In the process of heat storage, the electric energy consumed by the electric heating energy storage system varies according to the purchase price and the purchase cost. When the electric energy used by the electric heating energy storage system in the process of electric heating and heat storage comes from the wind abandonment power, the purchase cost of the wind abandonment power of the electric heating energy storage system can be expressed as:

$$C_{EH,3} = \sum_{t=1}^T p_w^t P_{wHE}^t \Delta T \quad (16)$$

If the heat stored by the electric heating energy storage system is not enough to supply the load demand of the heat network, and the power grid does not abandon wind at this time, it needs to purchase electric energy from the power grid for electric heating and heat storage. In this case, the purchasing cost of the electric heating energy storage system is generally higher than that of purchasing wind power abandonment. In this case, the corresponding normal purchasing cost of the electric heating energy storage system can be expressed as:

$$C_{EH,4} = \sum_{t=1}^T p_g^t P_{wHE}^t \Delta T \quad (17)$$

3.1.4. Cost Calculation of Heat Purchase for Electric Heating Energy Storage System

When the electric heating energy storage system is used as the heat source, if the power grid cannot provide enough electric energy for the electric heating energy storage system due to the limitation of peak regulation or operation regulation, it needs to purchase heat from other heat sources or heating plants to provide thermal peak regulation services for the electric heating energy storage system. Then, the heat purchase cost of the electric heating energy storage system when purchasing thermal peak regulation resources can be expressed as:

$$C_{EH,5} = p_h^t \sum_{t=1}^T P_{h2}^t \Delta T \quad (18)$$

3.2. Comprehensive Cost Model of Electric Hydrogen Energy Storage System

For the electric hydrogen energy storage system, its comprehensive cost can also be analyzed from three aspects: total system investment cost, maintenance cost, and efficiency cost of the electric hydrogen energy storage system.

3.2.1. Calculation of the Total Investment Cost of the Electric Hydrogen Energy Storage System

The total investment cost of the electric hydrogen energy storage system can be regarded as the fitting quadratic function between the total investment cost of the system and the input power of the system electric hydrogen production, the output power of the hydrogen fuel cell, and the energy storage capacity of the system, which can be expressed as:

$$\begin{aligned} C_{CH2ET,1} = & \alpha_{CH2E0} + \alpha_{CH2E11} P_{E2H} + \alpha_{CH2E21} P_{E2H}^2 \\ & + \alpha_{CH2E12} P_{H2E} + \alpha_{CH2E22} P_{H2E}^2 \\ & + \beta_{CH2E1} W_{H2SIN} + \beta_{CH2E11} W_{H2SIN}^2 \end{aligned} \quad (19)$$

3.2.2. Maintenance Cost Calculation of Electric Hydrogen Energy Storage System

The necessary maintenance of the electric hydrogen energy storage system after it is put into operation will generate certain expenses, which can be considered as proportional to the total investment cost of the system. Therefore, the maintenance cost of the electric hydrogen energy storage system can be expressed as:

$$C_{CH2ET,2} = C_{CH2ET,1} \cdot R_{CH2M} \quad (20)$$

3.2.3. Cost Calculation of Electro-Hydrogen Energy Storage Efficiency of Electric Hydrogen Energy Storage System

The electric hydrogen energy storage system includes three parts: electrolytic hydrogen production, hydrogen storage, and hydrogen fuel cell. Some energy is lost when electricity is converted to hydrogen energy using electrolytic hydrogen production equipment, and some energy is also lost when hydrogen fuel cells convert hydrogen energy into electricity. On the other hand, there will be energy loss in the process of injecting and releasing hydrogen into the hydrogen storage tank. Therefore, the energy loss of the electric hydrogen energy storage system consists of the four parts mentioned above. In a charge–discharge cycle, the ratio of the energy lost during the “electric energy—hydrogen energy—electric energy” conversion cycle to the electric energy absorbed by the electric hydrogen energy storage system in the electrolytic hydrogen production part is the energy loss ratio of the electric hydrogen energy storage system, which can be expressed as:

$$\mu_{H2SIN} = \frac{W_{H2INP} - W_{H2OUP}}{W_{H2INP}} \quad (21)$$

In Equation (21), the energy loss corresponding to the charge and discharge process of the electric hydrogen energy storage system is converted into electric quantity, and the corresponding electricity price is the cost of the electro-hydrogen energy storage efficiency of the electric hydrogen energy storage system.

Similar to the electric heating energy storage system and the electric vehicle, if the electric energy produced by the electric hydrogen energy storage system comes from wind power abandonment, the cost brought by energy storage efficiency can be expressed as:

$$C_{CH2ET,3} = \mu_{H2SIN} p_w^t \sum_{t=1}^T P_{wCH2}^t \Delta T \quad (22)$$

When electrolysis hydrogen production is performed in the non-wind abandoning condition due to the adjustment of its own operation mode, the electricity cost required is generally higher than the cost when purchasing wind abandoning power. In this case, the corresponding energy storage efficiency cost of electric hydrogen can be expressed as:

$$C_{CH2ET,3} = \mu_{H2SIN} p_g^t \sum_{t=1}^T P_{wCB}^t \Delta T \quad (23)$$

4. Carbon Emission Cost Model of Multi-Energy Power System

4.1. Carbon Emission Model of Coal-Fired Energy Supply

In the multi-energy power system, when the output of hydropower, wind power, photovoltaic, and other renewable energy sources as primary energy sources cannot meet the power load in the region, thermal power units need to bear the corresponding power load. At this time, coal combustion will inevitably bring about certain carbon dioxide emissions. Moreover, when the multi-energy power system needs to bear the heating load in the power supply area, if the electrothermal conversion device or the electric energy supply cannot meet all the heat energy supply, a certain amount of coal is needed for heating, which will also cause certain carbon dioxide emissions.

When the multi-energy power system is powered by burning coal, its corresponding carbon dioxide emissions can be expressed as:

$$CDE_{FUEL} = \mu_{CO2FUEL} \times CEF_{FUEL} \times TCC_{FUEL} \times ALCV_{FUEL} \times CCPU_{FUEL} \times COR_{FUEL} \quad (24)$$

According to the different values of coal quality consumed during coal-fired power supply in the power supply area of the multi-energy power system, the carbon emissions among different coals can be corrected.

4.2. Carbon Emission Cost Model of Coal-Fired Energy Supply

Whether coal-fired power supply of thermal power units or coal-fired heat supply of thermal power plants, coal-fired boilers are used to convert coal as a primary energy source into electricity or heat energy. The carbon emission cost of coal-fired energy supply is as follows:

$$CST_{RM} = \begin{cases} \alpha_i P_i^2 + \gamma_i P_i + \lambda_i + \delta_i \exp(\tau_i P_i) & P_b < P_i \leq P_{\max} \\ \alpha_i P_i^2 + \gamma_i P_i + \lambda_i + \delta_i \exp(\tau_i P_i) + k_c \text{oil}_{\text{cost}} & P_c < P_i \leq P_b \end{cases} \quad (25)$$

4.3. Carbon Transaction Cost of Multi-Energy Power System

The carbon emission quota of the multi-energy power system is:

$$CDE_{PSQU} = \eta_{PSQU} \sum_n \sum_t dPS_{n,t} \quad (26)$$

If the actual carbon emissions generated by the multi-energy power system are greater than the relevant carbon emission quota stipulated by the state, the multi-energy power system needs to purchase carbon emission rights in the carbon trading market, which is equivalent to increasing the operating cost. On the contrary, the energy and power system can sell carbon emission allowances to the carbon trading market and obtain corresponding income. Therefore, the carbon transaction cost of the multi-energy power system can be expressed as:

$$\begin{cases} CST_{MEPS} = EP_{CO2} (CDE_{MEPS} - CDE_{PSQU}) \\ CDE_{MEPS} = \alpha_{MEPS} \sum_m \sum_t dME_{m,t} \end{cases} \quad (27)$$

5. Multi-Objective Optimal Scheduling Model for Peak Regulation of Multi-Energy Power System

5.1. Optimization Objective

The optimal scheduling of the low-carbon economy for the multi-energy power system with the involvement of electricity, heat, and hydrogen, the multi-source energy storage system needs to consider the nonlinear relationship between the combination of a multi-energy power system peak regulating unit and multiple objectives, such as carbon emission, peak regulating economy, energy supply reliability, energy supply economy, and safety and stability, during the combination optimization process of multi-energy energy storage, thermal power, hydropower, wind power, and photovoltaic peak regulating unit. Therefore, in the optimization of the multi-energy power system, the combination of peak regulating units should satisfy multiple objective functions at the same time.

It is assumed that the multi-objective optimization scheduling model of the multi-energy power system has m optimization objective functions and n decision variables of maintenance unit combination optimization. Then, the model can be described as follows:

$$\begin{cases} \min & J_{BME} = f_{ME}(x) = (f_1(x), f_2(x), \dots, f_m(x)) \\ \text{s.t.} & g_{MEi}(x) \leq 0 (i = 1, 2, \dots, p) \\ & h_{MEj}(x) = 0 (j = 1, 2, \dots, q) \\ & x \in D \end{cases} \quad (28)$$

where x is the n -dimensional decision variable of the multi-objective optimal scheduling model for peak regulation of the multi-energy power system; $x = (x_1, x_2, \dots, x_i)$ is the i th decision variable for the optimal combination of peak regulating units in the multi-energy power systems; D is the n -dimensional decision space of the multi-objective optimal scheduling model for peak regulation of the multi-energy power system; J_{BME} is the objective function of the multi-objective optimal scheduling model for peak regulation of the multi-energy power system; $f_m(x)$ is the m th target component of the multi-objective optimal scheduling model for peak regulation of the multi-energy power system; $g_{MEi}(x)$ is p inequality constraints; $h_{MEj}(x)$ is q equality constraints.

To be specific:

The objective function of the multi-objective optimal scheduling model for peak regulation of the multi-energy power system includes the carbon emission cost of the multi-energy power system, the peak adjustment cost of a traditional synchronous power source, the peak adjustment cost of energy storage, the peak adjustment cost of new energy power source, the peak adjustment operating cost of flexible resources, and the deviation cost of the peak adjustment demand forecast of the multi-energy power system, which can be calculated as follows:

$$FMOP_1 \begin{cases} = \left[\begin{array}{l} \alpha_{CO2} P_{PERE}^2 + \gamma_{CO2} P_{PERE} \\ + \lambda_{CO2} + \delta_{CO2} \exp(\tau_{CO2} P_{PERE}) \end{array} \right] \Delta t \\ , P_{REMIN} < P_{PERE} \leq P_{REMAX} \\ = \left[\begin{array}{l} \alpha_{CO2} P_{PERE}^2 + \gamma_{CO2} P_{PERE} + \lambda_{CO2} \\ + \delta_{CO2} \exp(\tau_{CO2} P_{PERE}) + k_{CO2oil} P_{PERE} \end{array} \right] \Delta t \\ , P_{RELIM} < P_{PERE} \leq P_{REMIN} \end{cases} \quad (29)$$

$$FMOP_2 \begin{cases} = C_{PRS}(\beta_{REMIN} - \beta_{ROUT}) P_{PERE} \Delta t \\ , P_{REMIN} < P_{PERE} \leq P_{REMAX} \\ = C_{PRS}(\beta_{RELIM} - \beta_{ROUT}) P_{PERE} \Delta t \\ , P_{RELIM} < P_{PERE} \leq P_{REMIN} \end{cases} \quad (30)$$

When the electric heating energy storage system, the electric vehicle, and the electric hydrogen energy storage system participate in the peak regulating optimization of the multi-energy power system, some basic costs, such as construction investment depreciation and basic operation and maintenance of the energy storage system, need to be calculated in the peak adjustment cost, no matter whether energy storage is invoked in each dispatching time interval of actual operation. Therefore, the peak adjustment cost of energy storage in the multi-energy power system can be expressed as:

$$FMOP_3 = \left[\begin{array}{l} \left(\begin{array}{l} \alpha_{BUILD} C_{BUILD} + \alpha_{OPMN} C_{OPMN} \\ + \alpha_{PGEP} C_{PGEP} \end{array} \right) P_{PERE} \\ + \beta_{LDC0} + \beta_{LDC1} P_{PERE} + \beta_{LDC2} P_{PERE}^2 \end{array} \right] \Delta t \quad (31)$$

$$FMOP_4 = \beta_{RER0} C_{RER0} + \beta_{RER1} C_{PGEP} P_{PERE} \Delta t \quad (32)$$

$$FMOP_5 = (\beta_{UNR0} C_{UNR0} + \beta_{UNR1} C_{PGEP}) P_{\Delta PERE} \Delta t \quad (33)$$

5.2. Constraint Condition

5.2.1. Multi-Energy Power Balance Constraints

The constraint of multi energy power balance should meet the following formula:

$$\sum_{i=1}^{NG} (P_{MEGi}^{\Delta t} + P_{MESi}^{\Delta t} + P_{MELRi}^{\Delta t}) - \left[\sum_{j=1}^{NL} (P_{MELj}^{\Delta t} + P_{MESj}^{\Delta t} + P_{MELRj}^{\Delta t}) + \sum P_{LS}^{\Delta t} \right] = 0 \quad (34)$$

where Δt is a certain period of operation of the multi-energy power system; $P_{MEGi}^{\Delta t}$ is the output value of each equivalent power source in the first period Δt of the multi-energy power system; $P_{MESi}^{\Delta t}$ and $P_{MESj}^{\Delta t}$ are the power values of electricity storage, heat storage, and hydrogen storage in the discharge and charge states in the multi-energy power system, respectively; $P_{MELRi}^{\Delta t}$ and $P_{MELRj}^{\Delta t}$ are the power values of electricity, heat, and hydrogen demand, responding to load to reduce the load demand and increase the load demand in the multi-energy power system, respectively; $P_{MELj}^{\Delta t}$ is the equivalent multi-energy load value of the multi-energy power system in the period Δt ; $\sum P_{LS}^{\Delta t}$ is the total active network loss corresponding to multi-energy transmission in the first period Δt of the multi-energy power system.

$$\sum P_{LS}^{\Delta t} = \sum_{i=1}^n \sum_{j=1}^n P_{MEi}^{\Delta t} B_{ij} P_{MEj}^{\Delta t} \quad (35)$$

where B_{ij} is the receptivity between nodes i and j in the multi-energy power system network; $P_{MEi}^{\Delta t}$ and $P_{MEj}^{\Delta t}$ are the total calculated power of multi-energy on nodes i and j in the multi-energy power system network, respectively.

5.2.2. Constraints on the Scope of Flexible Resource Regulation

Various regulatory resources should meet the following constraints:

$$\begin{cases} P_{MEGi,\min}^{\Delta t} \leq P_{MEGi}^{\Delta t} \leq P_{MEGi,\max}^{\Delta t} \\ P_{MESi,\min}^{\Delta t} \leq P_{MESi}^{\Delta t} \leq P_{MESi,\max}^{\Delta t} \\ P_{MELRi,\min}^{\Delta t} \leq P_{MELRi}^{\Delta t} \leq P_{MELRi,\max}^{\Delta t} \end{cases} \quad (36)$$

where $P_{MEGi,\min}^{\Delta t}$ and $P_{MEGi,\max}^{\Delta t}$ are the upper and lower limits of the adjustment ranges of thermal power, hydropower, and new energy power in the multi-energy power system within the time period Δt , respectively; $P_{MESi,\max}^{\Delta t}$ and $P_{MESi,\min}^{\Delta t}$ are the upper and lower limits of charging and discharging power of electric storage, hydrogen storage, and heat storage systems in the multi-energy power system during the time period Δt , respectively; $P_{MELRi,\min}^{\Delta t}$ and $P_{MELRi,\max}^{\Delta t}$ are, respectively, the adjustable upper and lower limits of the demand-side response power of electricity, hydrogen, and heat loads in the multi-energy power system during the time period Δt .

5.2.3. Constraints on the Characteristics of Flexible Resource Regulation Response

According to the peak regulation requirements of the multi-energy power system, the climbing rate of flexible resources involved in peak regulation can be expressed by the climbing rate of power regulation characteristics and the climbing rate of power regulation characteristics.

$$\begin{cases} \frac{P_{MEGi}^t - P_{MEGi}^{t-\Delta t}}{\Delta t} \leq D_{UPRi} \\ \frac{P_{MEGi}^{t-1} - P_{MEGi}^t}{\Delta t} \leq D_{DNRi} \end{cases} \quad (37)$$

where D_{UPRi} is the climbing rate of the i th flexible resource participating in peak regulation of the multi-energy power system; D_{DNRi} is the downhill climbing rate of the i th flexible resource participating in peak regulation of the multi-energy power system; P_{MEGi}^t is the

output value of the i th flexible resource participating in peak regulation of the multi-energy power system at time t .

5.2.4. Reserve Constraint of Forecasting Deviation in Peak Regulating Demand

In the actual operation of the multi-energy power system, the errors in the forecast of the demand for peak regulating capacity required in each dispatching time interval in the future and the problems, such as the failure and maintenance of flexible resource equipment involved in peak regulating, will lead to deviation between the predicted peak regulating capacity and the actual demand for peak regulating. Therefore, the upper and lower reserve constraints of the forecasting deviation of peak regulating demand can be expressed as:

$$\begin{cases} \sum_{i=1}^N R_{MEui}^t \geq R_{MED}^t + u_{UPMEs} P_{PERE} \\ R_{MEui}^t = \min(P_{MEGi,max}^t - P_{MEGi}^t, D_{UPRi} \Delta t) \end{cases} \quad (38)$$

$$\begin{cases} \sum_{i=1}^N R_{MEdi}^t \geq u_{DNMEs} P_{PERE} \\ R_{MEdi}^t = \min(P_{MEGi}^t - P_{MEGi,min}^t, D_{DNRi} \Delta t) \end{cases} \quad (39)$$

where R_{MEui}^t is the upper capacity of the flexibility resources for peak regulation provided by unit i at time t within the scheduling time interval; R_{MED}^t represents the standby capacity of the multi-energy power system on peak regulation at time t in view of the demand prediction error of peak regulation capacity and the outage of flexible resources of peak regulation; u_{UPMEs} is the ratio coefficient of error prediction for the upper reserve capacity demand of the multi-energy power system peak regulating resources, which can range from 10 to 30% for different dispatching time intervals; R_{MEdi}^t is the lower capacity of unit i under the flexibility resource of peak regulation at time t within the scheduling time interval; u_{DNMEs} is the proportional coefficient of error in prediction of reserve capacity demand under peak regulating resources of the multi-energy power system, which can range from 10 to 30% for different dispatching time intervals.

5.2.5. Electric Vehicle Charging and Discharging Constraints

In order to extend the service life of electric vehicle batteries, it is necessary to limit the maximum and minimum battery power of electric vehicle batteries.

$$\begin{aligned} S_{OCmin} &\leq S_{OC,t} \leq S_{OCmax} \\ S_{OC,t} &= S_{OC,t-1} + \Delta t P_{CH,t} \eta_{CH} - \\ &\quad \Delta t P_{DIS,t} / \eta_{DIS} - (1 - \rho_t) E_V D_{PC} \end{aligned} \quad (40)$$

where: $S_{OC,t}$ represents the overall remaining power of all electric vehicles during period t ; S_{OCmax} represents the maximum value of the overall battery power; S_{OCmin} represents the minimum value of the overall battery power; D_{PC} represents the average power consumption of an electric vehicle for 1 h.

5.3. Solving Algorithm

In this paper, the NSGA-II algorithm is used to solve the multi-objective optimal scheduling model for peak regulation of the multi-energy power system. The specific process is as follows:

The number of objective functions of the multi-objective optimal scheduling model for peak regulation of the multi-energy power system is set as m . The initial population amount of flexible resource peak regulating unit combination participating in peak regulating optimal scheduling of the multi-energy power system is N . The number of elite solutions of flexible resource peaking unit combination is $N/2$. The maximum number of function calls is CFI_{max} . The dimension of decision variable peak shaving unit combination is j . The upper and lower bounds of the decision variables of the flexible resource peak shaving unit

combination participating in the peak shaving optimal scheduling of multi-energy power systems are $\mu_{TOP} = (\mu_1, \mu_2, \dots, \mu_i, \dots, \mu_j)$ and $l_{BOT} = (l_1, l_2, \dots, l_i, \dots, l_j)$, respectively. The shape parameter is set to β . The crossover parameter of the flexible resource peaking unit combination population is θ_c , and its crossover probability is p_c . The population mutation parameter of flexible resource peaking unit combination is θ_m , and its mutation probability is p_m .

Step 1: initialize the flexible resource peaking unit combination population $p = (p_1, p_2, \dots, p_n, \dots, p_N)$, and calculate the objective function value corresponding to each flexible resource unit in the flexible resource peaking unit combination population, where $p_n = (x_1, x_2, \dots, x_i, \dots, x_j)$ and $n = 1, 2, \dots, N, x_i \in (l_{BOT}, \mu_{TOP})$.

Step 2: the solutions in the flexible resource peak regulating unit commitment population $p = (p_1, p_2, \dots, p_n, \dots, p_N)$ are sorted in a non-dominated way. After sorting, all non-dominated solutions of the current flexible resource peak shaving unit commitment population are recorded as p_C .

Step 3: the current flexible resource peaking unit combination population p_C is mapped to the hyperplane HS_{MEC} , corresponding to the optimal scheduling objective function value, and the matrix mapped by the current flexible resource peaking unit combination population p_C is p'_C .

Step 4: the crowding distance of the current flexible resource peaking unit commitment population p'_C is calculated and sorted according to the non-dominated solution value and the crowding distance. After sorting, the flexible resource peaking unit commitment population is recorded as NRP .

Step 5: the flexible resource peaking unit combination population after sorting is mutated and enhanced, and the mutated flexible resource peaking unit combination population p_E is obtained.

Step 6: remove the individuals contained in p_E in the flexible resource peaking unit combination population p_C and then select $\frac{N}{2} - n\max(nr)$ flexible peaking unit individuals according to the crowding distance, which is recorded as p_S .

Step 7: the flexible resource peak shaving unit combination population p_E and p_S are merged to obtain the flexible resource peak shaving unit combination population p_M , and then the p_M is cross-mutated to obtain a new flexible resource peak shaving unit combination population p_H . Finally, the peak shaving unit combination populations p_H and p_M are merged into the next generation of flexible resource peak shaving unit combination population p_{NG} ;

Step 8: repeat the above steps 2 to step 7. When the maximum number of generations is reached or the preset target is reached, the non-dominated solution in the current flexible resource peaking unit combination population p_{NG} is the optimal solution of the multi-energy power system peaking low-carbon economy optimal scheduling unit combination.

The process of variation enhancement is as follows:

$$\begin{cases} p_{ME-nrm}^*(k) = (p'_{ME-nrm1}, \dots, p'_{ME-nrmi}, \dots, p'_{ME-nrmj}) \\ p'_{ME-nrmi} = \lambda p_{ME-nrmi} \\ 0 < i \leq j \\ k = 1, 2, \dots, \eta N_{ME-\mu} \end{cases} \tag{41}$$

where $p_{ME-nrm}^*(k) = (p'_{ME-nrm1}, \dots, p'_{ME-nrmi}, \dots, p'_{ME-nrmj})$ is the assumed current selected individual; j is the number of decision variables; N_{ME} is the total population of flexible resource peaking units; $N_{ME-\mu}$ is the number of local solutions of flexible resource peak shaving unit commitment, which is determined by the dynamic change in the flexible resource peak shaving unit commitment solution in the iterative process; $\lambda \in (1, 2)$ is a random number; $\eta \in (0, 1)$ is a variation parameter set according to the peak regulation demand characteristics of the multi-energy power system and the corresponding flexible peak regulation resource characteristics.

When the distribution of the flexible resource population is not ideal, $(1 + \eta)\lambda$ a local flexible resource peak shaving unit combination solution can be generated in the flexible resource classification area with poor distribution through Equation (38), which effectively improves the distribution of the solution in the peak shaving unit combination solution process.

Figure 1 is a flow chart of the NSGAI algorithm for the distribution of low-carbon economic dispatch in a multi-energy power system.

In this paper, the fuzzy evaluation method is used to obtain the optimal compromise solution between multiple objectives. Firstly, the single objective function value of each individual can be fuzzified according to the following membership function:

$$\mu_{\zeta} = \begin{cases} 1, & F_{\zeta} \leq F_{\zeta,\min} \\ \frac{F_{\zeta,\max} - F_{\zeta}}{F_{\zeta,\max} - F_{\zeta,\min}}, & F_{\zeta,\min} \leq F_{\zeta} \leq F_{\zeta,\max} \\ 0, & F_{\zeta} \geq F_{\zeta,\max} \end{cases} \quad (42)$$

where F_{ζ} is the function value of the first objective; $F_{\zeta,\min}$ and $F_{\zeta,\max}$ are the minimum and maximum values of the first target, respectively.

The fuzzified single objective function value is weighted and summed according to the target weight preference, that is,

$$\mu = \frac{1}{M} \sum_{\zeta=1}^M \mu_{\zeta} \quad (43)$$

where μ is the value of satisfaction; M is the number of objective functions to be optimized.

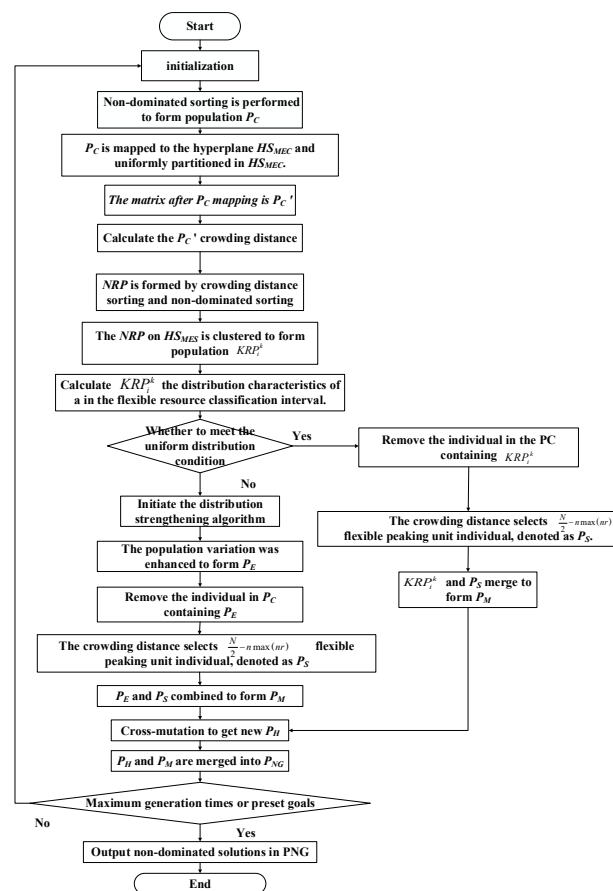


Figure 1. Flow chart of NSGAI algorithm for enhancing the distribution of peak shaving and low-carbon economic dispatching in multi-energy power system.

6. Simulation

Taking the data of a county-level power grid in Northeast China as the basic data source, a multi-energy power system model including new energy sources represented by wind, solar and power generation, electric heating energy storage system, electric vehicle, electric hydrogen energy storage system, thermal power unit, and other flexible adjustment resources is built for the simulation analysis in this paper. In Tables 1 and 2, the relevant parameters of flexible adjustment resources for various types of energy forms, such as wind power, photovoltaic, thermal power, heat storage, power storage, hydrogen storage, and so on, are given, respectively.

In the multi-objective optimization model algorithm proposed in this paper, the population size is 100, the maximum number of iterations is 200, the crossover probability is 0.7, the mutation probability is 0.5, and the crossover and mutation parameters are both 20.

Table 1. Related parameters of the system generator.

Power Type	Power Capacity (MW)
Wind power	200 MW
Photovoltaic	160 MW
Thermal power	120 MW

Table 2. Related parameters of various energy storage devices.

Energy Storage Type	Charging Efficiency	Energy Release Efficiency	Energy Storage Capacity (MW)
Electric heating energy storage system	80%	80%	60
electric vehicle	85%	85%	120
Electric hydrogen Energy Storage System	50%	50%	70

Figure 2 shows the topology structure of the simulation system. This system includes equipment such as electric boilers, heat storage, fuel cells, and hydrogen production.

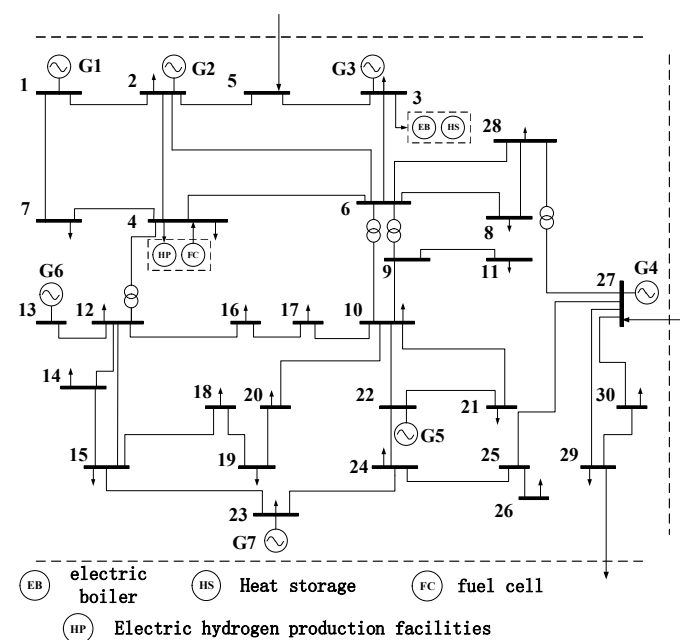


Figure 2. Topological structure diagram of the simulation system.

Figure 3 shows the output of each power source in the multi-energy power system on a typical day. Figure 4 shows the comprehensive peak regulation demand of electricity, heat, and hydrogen load in the multi-energy power system equivalent to the peak regulation demand of electricity. Figure 5 shows the uncertainty of the output and load of each power source in the system.

According to the typical output and its uncertainty curve in the multi-energy power system in Figures 3 and 4, combined with the multi-objective optimal scheduling model and solution algorithm of the multi-energy power system peak regulation established in this paper, the simulation analysis is carried out.

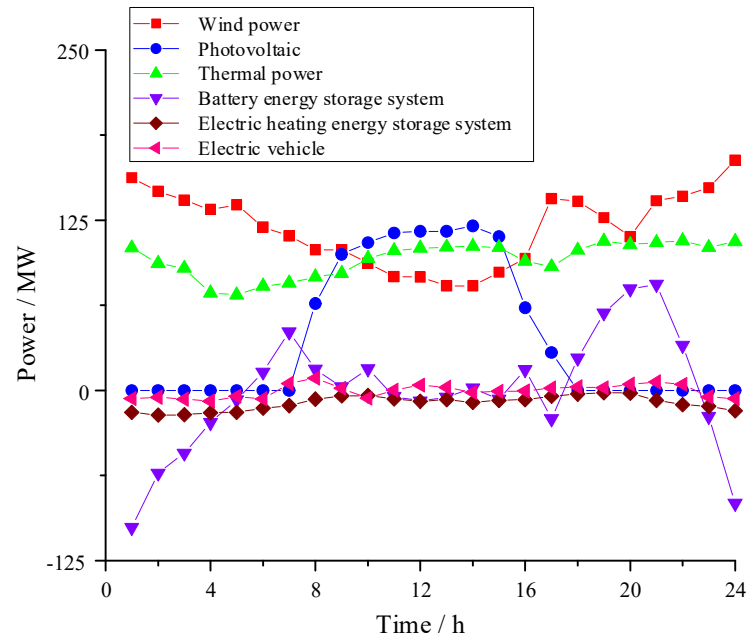


Figure 3. Typical output of multi-energy power system.

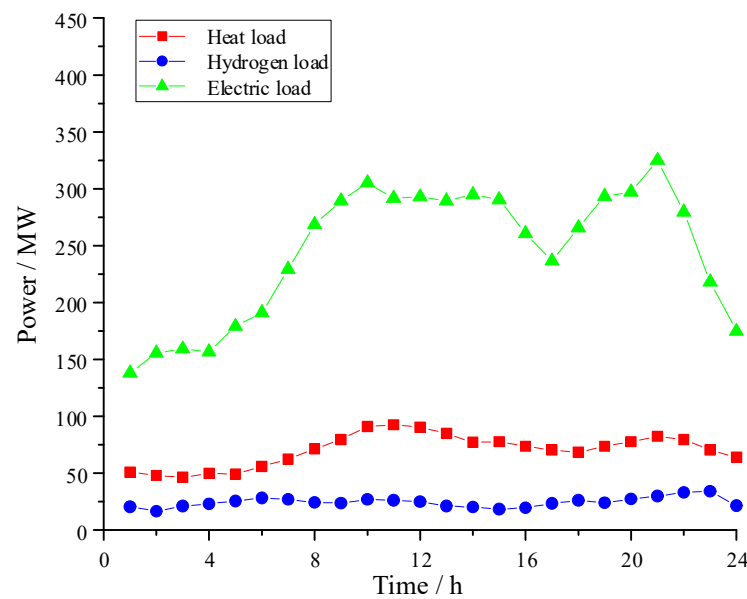


Figure 4. Peak load regulating demand of electricity, heat, and hydrogen.

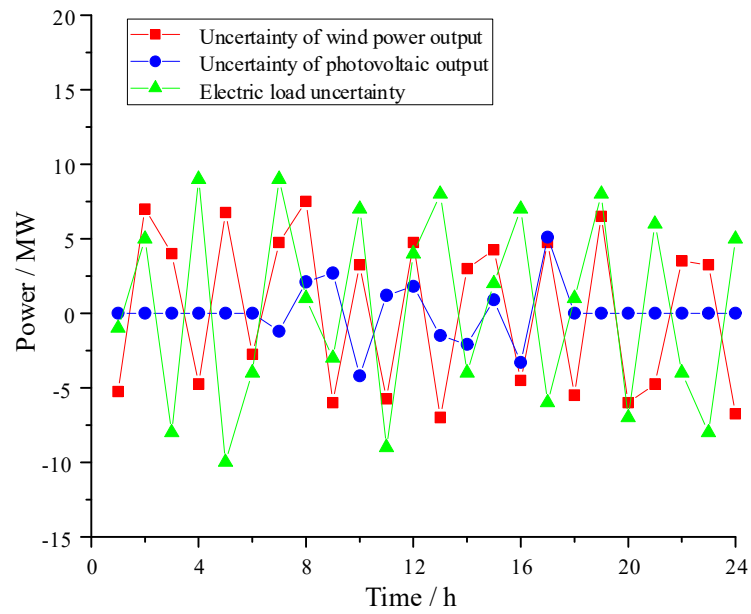


Figure 5. Typical output uncertainty of the system.

Figure 6 shows the flexibility resource capacity allocation curve of the optimized multi-energy power system under the peaking demand and its uncertainty scenario in Figure 4. The corresponding combinations of wind power, photovoltaic, thermal power, heat storage, electricity storage, and hydrogen storage peak regulating units are shown in Figure 7.

It can be seen from the diagram that on the basis of considering the energy balance demand, peak shaving demand, and carbon emission cost optimization demand of the multi-energy power system, the start-up mode and peak shaving reserve capacity of thermal power units in peak shaving optimization scheduling of the multi-energy power system are further reduced.

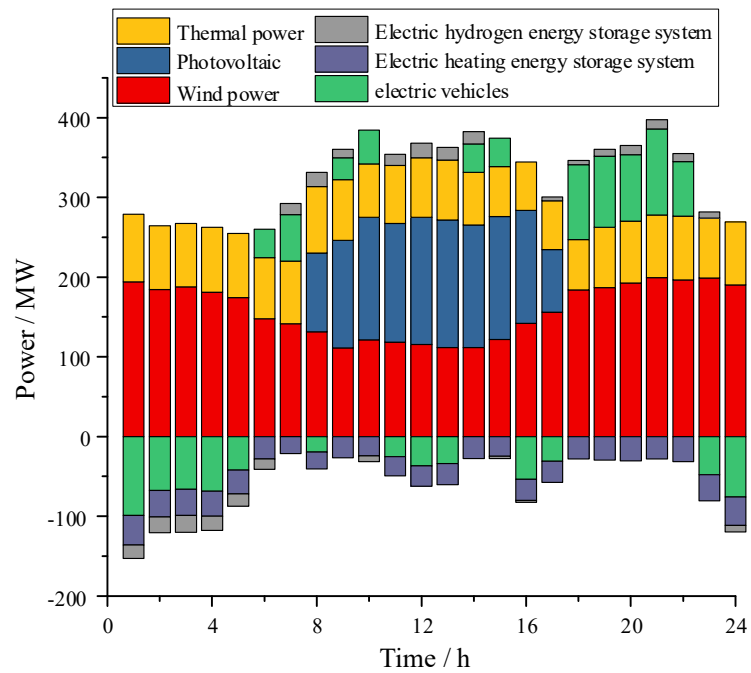
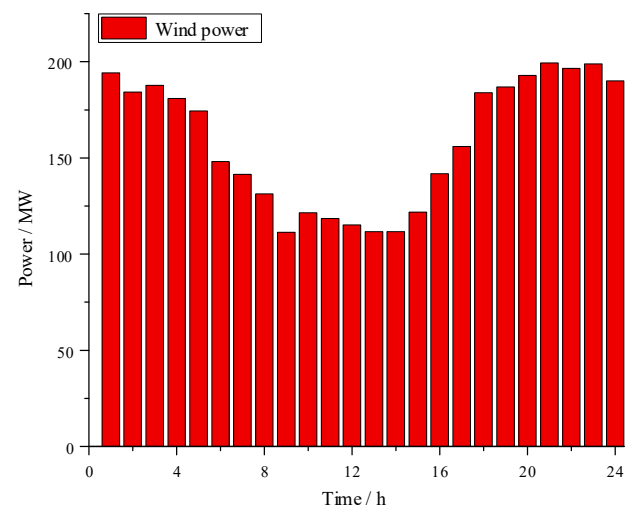
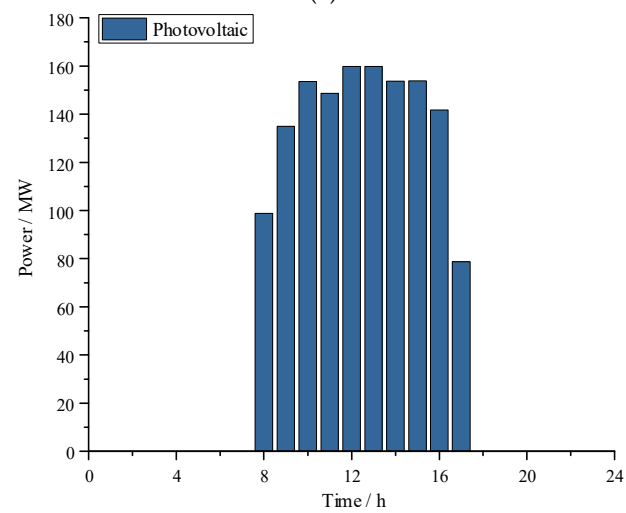


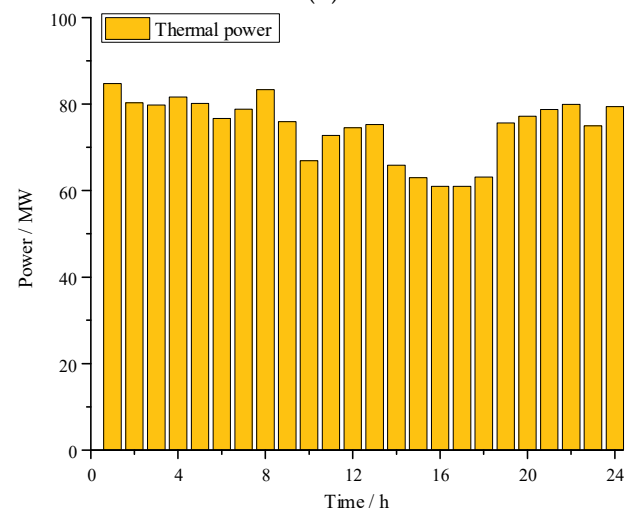
Figure 6. Capacity allocation curve of the system flexibility resource.



(a)

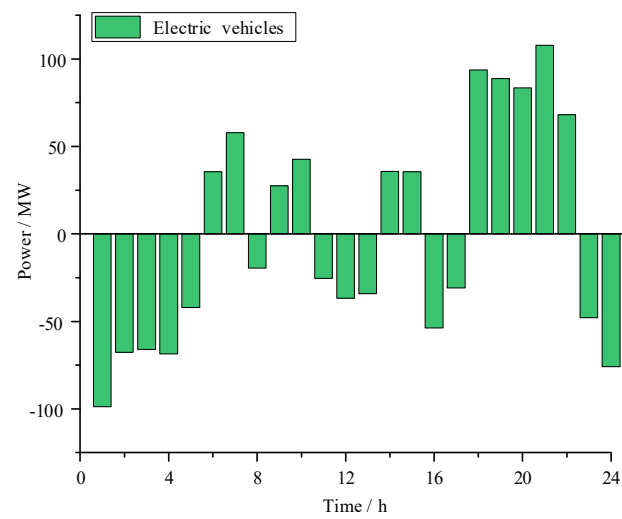


(b)

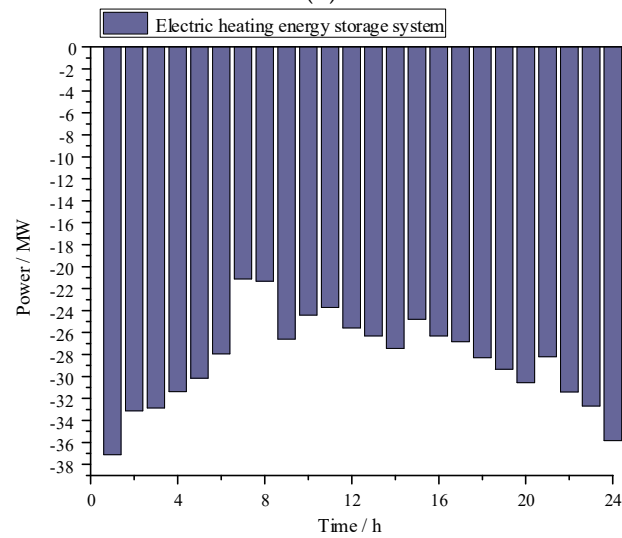


(c)

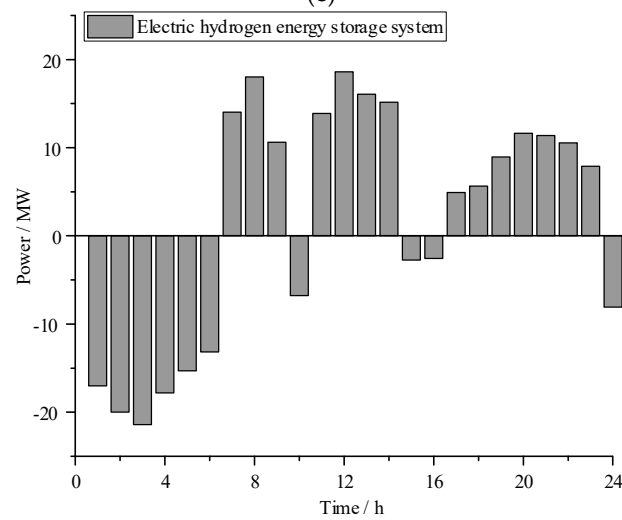
Figure 7. Cont.



(d)



(e)



(f)

Figure 7. Combination of peak regulating unit. (a) Wind power; (b) photovoltaic; (c) thermal power; (d) electric vehicle; (e) electric heating energy storage system; (f) electric hydrogen energy storage system.

Correspondingly, according to the flexible resource carbon emission and economic cost model participating in peak shaving, the carbon emission curve, carbon emission cost, and economic cost of multi-energy power system peak shaving can be obtained, respectively, as shown in Figures 8 and 9.

Combined with Figures 7–9, it can be found that because the solution process of the optimal scheduling model effectively avoids the singleness of the population and the irrationality of the energy type, the energy type is effectively and flexibly selected according to the peak shaving demand and operating cost in the solution process. Therefore, the multi-objective optimal scheduling model of the multi-energy power system can effectively take into account the coordination characteristics of multi-energy and the distribution characteristics of flexible peak shaving resources while making full use of the coordination between the electrothermal energy storage system, electric vehicle, and electro-hydrogen energy storage system. While reducing the peak shaving carbon emissions and economic costs of multi-energy power systems, it also improves the peak shaving performance and new energy consumption level of the multi-energy power system.

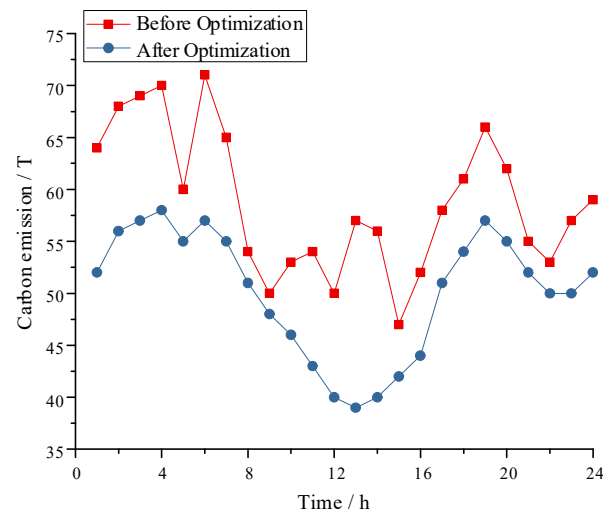


Figure 8. System carbon emission change curve.

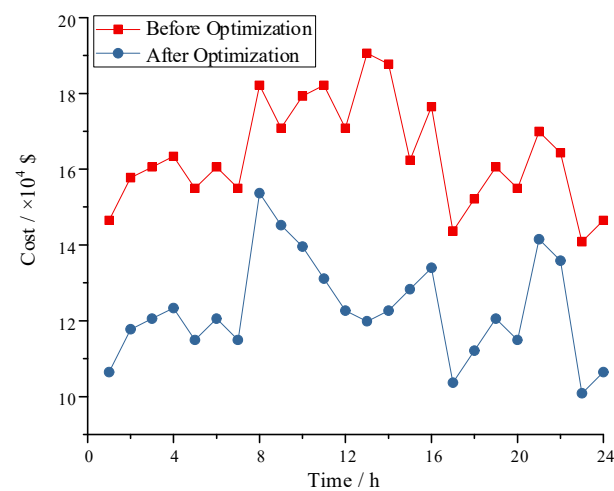


Figure 9. System carbon emission cost and economic cost curve.

After considering the low-carbon optimization scheduling model for peak shaving resources in the multi-energy power system proposed in this article, sufficient load reserve and power balance disturbance reserve can be provided at a lower cost. Meanwhile, according to Table 3, it can be seen that although the peak shaving cost of energy storage

and new energy sources is higher than before optimization, the deviation cost of peak shaving demand prediction for multi-energy power systems is lower, resulting in lower total costs.

Table 3. Comparison of cost optimization results/ 10^4 USD.

	Before Optimization	After Optimization
Carbon emission cost of multi energy power systems	13.13	6.12
Peak shaving cost of traditional synchronous power supply	243.8288	140.4215
Peak shaving cost of energy storage	72.837	101.136
Peak shaving cost of new energy sources	39.356	49.907
Bias cost of peak shaving demand prediction in multi energy power systems	212.9002	131.012
total cost	582.052	428.5965

7. Conclusions

Based on the comprehensive cost of multi-energy storage and the calculation model of carbon emission cost of peak regulating resources of the multi-energy power system, the multi-objective optimal scheduling model for peak regulation of the multi-energy power system that considers the demand of “carbon reduction” is studied and established. The following conclusions are obtained.

- (1) From the aspects of investment construction, operation maintenance, and operation efficiency of the electric heating energy storage system, the electric vehicle, and the electric hydrogen energy storage system, a comprehensive cost calculation method of the multi-energy power system energy storage is proposed, and an accurate analysis of the operation peak adjustment cost of the multi-energy storage participating in the peak adjustment system is realized.
- (2) The optimal scheduling method of peak regulation resources for the multi-energy power system is proposed, which not only considers the economy of peak regulation of the multi-energy power system but also considers the demand of carbon emission reduction in the system, thus achieving reductions in the carbon emission cost of the system.
- (3) The optimal scheduling of peak regulating resources can also help to improve the level and capacity of the energy storage system and new energy units in a multi-energy power system to participate in peak regulating, improving the level of new energy consumption in the system.

In future research, we will be able to quickly and accurately determine the local area or node in the multi-energy power system with energy imbalance and the energy form of its energy regulation demand for the multi-energy power system under different peak regulation capacity requirements and different energy forms. Based on the state perception of the multi-energy power system, the energy control of different energy forms in the multi-energy power system is the next step study.

Author Contributions: Conceptualization, K.Z. and Z.C.; methodology, K.D.; software, K.D.; validation, K.D., J.L. and L.L.; writing—original draft preparation, K.D.; writing—review and editing, K.D.; visualization, P.S. All authors have read and agreed to the published version of the manuscript.

Funding: This research was funded by the National Key Research and Development Program of China (No. 2017YFB0902100).

Data Availability Statement: The simulation analysis part of this article is based on real operating power grid data, and for confidentiality reasons, the data in this article will not be disclosed.

Conflicts of Interest: The authors declare no conflict of interest.

Nomenclatures

P_{EVmin}, P_{EVmax}	the lower limit and upper limit of the total charging and discharging power of the electric vehicle during the t period
ρ_t	the driving and stopping probability of electric vehicles during the t period
E_V	the total number of electric vehicles
P_{DIS}	the discharge power of a single electric vehicle
P_{CH}	the charging power of a single electric vehicle
η_{DIS}, η_{CH}	the discharging and charging efficiency of an electric vehicle
$C_{CBTN,1}$	the total investment cost of electric vehicle
P_{BSIN}	the charging and discharging power of the electric vehicle
W_{BSIN}	the storage capacity of electric vehicle
$\alpha_{CB0}, \alpha_{CB1}, \alpha_{CB2}, \beta_{CB1}, \beta_{CB2}$	the fitting coefficient of the total investment cost of the electric vehicle
Y_{kcdc}	the capacity attenuation function of chemical battery in the electric vehicle
λ_B	the battery type constant in the electric vehicle, which is used to describe the corresponding attenuation rate of batteries with different electrolyte types and ion types
W_{ACE}	battery activation energy in electric vehicle
T_{emp}	the battery temperature in the electric vehicle
R_{SEI}	the gas constant
ζ	the power law relation index
k_{CDC}	the number of charge and discharge cycles of the battery in the electric vehicle
ϕ_{CDC}	the difference between the charging and discharging power of the electric vehicle and the rated power
P_{INP}	the actual charging and discharging power of batteries in the electric vehicle
P_{BSIN}	the rated charging and discharging power of the battery in the electric vehicle
$\varphi(k_{CDC})$	the influence coefficient of single charge and discharge power of electric vehicle on battery capacity attenuation
SOH_{CB}	the battery performance state of the electric vehicle
W_{NOM}	the nominal capacity of the electric vehicle
$C_{CBTN,2}$	the performance degradation cost corresponding to a single charge–discharge cycle of the electric vehicle
$\vartheta_{BSP1}, \vartheta_{BSP2}$	the purchase cost coefficient of battery itself
$C_{CBTN,3}$	the maintenance cost of electric vehicle
R_{CBm}	the proportion of maintenance cost of electric vehicle.
μ_{BSIN}	the energy loss rate of electric vehicle
W_{INP}, W_{OUP}	the input energy and output energy of the electric vehicle.
$C_{CBTN,4}$	the battery energy storage efficiency cost of the electric vehicle
p_w	the electricity price of the grid when the electric vehicle is storing electric energy
P_{wCB}^t	the energy storage power of the electric vehicle
ΔT	the operation time of the electric vehicle under the energy storage state.
p_g^t	the grid non-wind abandoning price when the electric vehicle carries out electric energy storage.
$C_{EH,1}$	the total investment cost of the electric heating energy storage system;
	the cost of equipment resistance heater, the cost of system heat storage body, the cost of gas-water heat exchange equipment, the cost of equipment insulation layer, the cost of high-voltage control cabinet, the cost of other auxiliary equipment, the cost of land occupation and the construction cost in the total investment cost of the electric heating energy storage system.
$C_{he}, C_{hs}, C_{ts}, C_{il}, C_{hv}, C_{el}, C_{gr}, C_{cn}$	

$\overline{P_{ein}}$	the electric heating power
$\overline{a_0, a_1, a_2}$	the corresponding cost coefficient
$\overline{C_{ph}}$	heat storage capacity
$\overline{b_0, b_1, b_2}$	the corresponding cost coefficients
$\overline{P_{hout}}$	output power of the electric heating energy storage system
c_0, c_1, c_2	the corresponding cost coefficients
S_{ps}	external area of the electric heating energy storage system equipment
p_{ps}	the cost of thermal insulation material per unit area of the system equipment;
V_{ps}	the volume of the system heat storage body;
c_{sh}	the heat storage density of the system heat storage body;
ρ_{ph}	the density of the system heat storage body;
k_{ps}	the margin coefficient of the system heat storage body
h_{ph}, w_{ph}	the height and width of the system heat storage body respectively;
d_0, d_1	the corresponding cost coefficient of C_{hw}
e_0, e_1, e_2	represent the corresponding cost coefficients of C_{el}
g_0, g_1, g_2	the corresponding cost coefficients of C_{gr}
h_0, h_1, h_2	the corresponding cost coefficients of C_{cn}
$a_{00}, a_{11}, a_{22}, b_{11}, b_{22}$	the fitting coefficient of the total investment cost.
$C_{EH,2}$	the maintenance cost of the electric heating energy storage system
R_m	the proportion of maintenance cost.
$C_{EH,3}$	where $C_{EH,3}$ represents the purchasing cost of wind power abandonment of the electric heating energy storage system;
p_w^t	the wind abandonment price of the power grid;
P_{wHE}^t	the corresponding electric power of the electric heating storage system;
$C_{EH,4}$	the purchasing cost of wind power abandonment of the electric heating energy storage system;
p_g^t	the wind discard price of the power grid.
$C_{EH,5}$	the heat purchase cost of thermal peak regulation resources purchased by the electric heating energy storage system
p_h^t	the unit price of heat for other heat sources or heating plants
P_{h2}^t	the heating support power provided by other heat sources or heating plants for the electric heating energy storage systems.
$C_{CH2ET,1}$	the total investment cost of the electric hydrogen energy storage system;
P_{E2H}	the input power of electro-hydrogen production in the electric hydrogen energy storage system;
P_{H2E}	the output power of hydrogen fuel cell of the electro-hydrogen energy storage system;
W_{H2SIN}	the energy storage capacity of the electric hydrogen energy storage system.
$C_{CH2ET,2}$	the maintenance cost of the electric hydrogen energy storage system;
R_{CH2M}	the proportion of maintenance cost of the electric hydrogen energy storage system.
μ_{H2SIN}	the energy loss ratio of the electric hydrogen energy storage system;
W_{H2INP}, W_{H2OUP}	the energy input and output of the electric hydrogen energy storage system.
$C_{CH2ET,3}$	the efficiency cost of the electric hydrogen energy storage system;
p_w^t	the power grid wind abandon price during electrolytic hydrogen production;
P_{wCH2}^t	the electrolytic hydrogen production power of the electric hydrogen energy storage system
p_g^t	the non-wind curtailment price of the grid.

CDE_{FUEL}	the carbon dioxide emission in the process of burning coal for energy supply;
CE_{FUEL}	the carbon emission factor of coal consumed in the process of coal-fired energy supply;
TCC_{FUEL}	the total coal consumption for coal-fired power supply process;
$ALCV_{FUEL}$	the average low calorific value of coal consumed in the process of coal-fired energy supply
$CCPU_{FUEL}$	the carbon content per unit calorific value of coal consumed in the process of coal-fired energy supply
COR_{FUEL}	the carbon oxidation rate of coal consumed in coal-fired energy supply process
$\mu_{CO2FUEL}$	the correction coefficient of coal quality difference in the process of coal-fired power supply.
CST_{RM}	the carbon emission cost of the coal-fired power supply;
$\alpha_i, \gamma_i, \lambda_i, \delta_i, \tau_i$	the carbon emission parameter of the coal-fired boiler;
P_i	equivalent output power of the coal-fired boiler;
k_c	the carbon emission corresponding to fuel combustion per unit weight
oil_{cost}	the fuel consumption of the coal-fired boiler under the operation mode of oil injection depth adjustment;
P_{max}	the maximum equivalent output power of the coal-fired boiler under the conventional regulation operation mode;
P_b	the minimum equivalent output power of the coal-fired boiler under the operation mode of no oil injection depth adjustment;
P_c	the minimum equivalent output power of the coal-fired boiler under the operation mode of adjusting the oil injection depth.
CDE_{PSQU}	the carbon emission quota of multi-energy power system;
η_{PSQU}	the carbon emission quota per unit electricity quantity of the multi-energy power system;
$dPS_{n,t}$	the equivalent electric load power actually consumed by network node
n	the multi-energy power system at time
CST_{MEPS}	the carbon transaction cost of the multi-energy power system;
CDE_{MEPS}	the actual total carbon emissions of the multi-energy power systems
EP_{CO2}	the carbon price of the multi-energy power system at time t ;
$dME_{m,t}$	the output of coal-fired boiler m of the multi-energy power system at time t ;
α_{MEPS}	the carbon dioxide emission coefficient of coal consumed by coal-fired boilers in the multi-energy power systems.
$FMOP_2$	the peak adjustment cost of traditional synchronous power supply;
C_{PRS}	the price of primary energy consumed by traditional synchronous power sources such as hydroelectric, thermal or nuclear power units;
$\beta_{ROUT}, \beta_{REMIN}, \beta_{RELIM}$	the primary energy consumption coefficient of traditional synchronous power supply, the primary energy consumption coefficient under rated working conditions and the primary energy consumption coefficient below the output reduction limit;
P_{PERE}	the peak regulating power demand of multi-energy power system in a time scale;
P_{REMIN}, P_{REMAX}	the upper and lower limits for normal adjustment of traditional synchronous power sources such as hydroelectric, thermal or nuclear power units;
P_{RELIM}	the output reduction limit of traditional synchronous power sources such as hydroelectric, thermal or nuclear power units.

$FMOP_3$	the peak adjustment cost of energy storage in the multi-energy power system;
$C_{BUILD}, C_{OPMN}, C_{PGEP}$	the investment cost of the multi-energy storage system construction, basic operation and maintenance cost, and the corresponding electricity price within the time scale;
$\alpha_{BUILD}, \alpha_{OPMN}, \alpha_{PGEP}$	the depreciation coefficient of investment cost, basic operation and maintenance cost and power purchase cost of multi-energy storage system;
$\beta_{LDC0}, \beta_{LDC1}, \beta_{LDC2}$	life attenuation coefficient of multi-energy storage system; P_{PERE} is the peak regulating power demand of multi-energy power system in a time scale Δt .
$FMOP_4$	the peak adjustment cost of energy storage in the multi-energy power system;
C_{RERO}	the basic operation cost composed of the investment depreciation and operation and maintenance cost of the new energy power supply participating in peak regulation during the grid-connected operation;
β_{RERO}	the peak adjustment cost coefficient of new energy power supply participating in peak adjustment under the corresponding basic operation cost;
C_{PGEP}	the corresponding electricity price within the time scale Δt ;
β_{RER1}	the cost coefficient of electricity price when new energy power supplies participate in peak regulation;
P_{PERE}	the peak regulating power demand of the multi-energy power system in time scale Δt .
$FMOP_5$	the forecast deviation cost of peak regulating demand for the multi-energy power system;
$P_{\Delta PERE}$	the power prediction deviation of peak regulating demand considered when optimizing the combination of peak regulating units in a multi-energy power system;
C_{UNRO}	the unit cost corresponding to the purchase of standby capacity of peak regulation for multi-energy power system;
β_{UNRO}	the backup cost coefficient of multi-energy power system purchase of peak regulation;
C_{PGEP}	the corresponding electricity price in the time scale Δt ;
β_{UNR1}	the power cost coefficient of the standby peak-regulating unit caused by more or less power generation in time scale Δt .

References

- Zhou, X.; Zhao, Q.; Zhang, Y.; Sun, L. Integrated energy production unit: An innovative concept and design for energy transition toward low-carbon development. *CSEE J. Power Energy Syst.* **2021**, *7*, 1133–1139.
- Gutierrez-Martinez, V.; Moreno-Bautista, C.; Lozano-Garcia, J.; Pizano-Martinez, A.; Zamora-Cardenas, E.A.; Gomez-Martinez, M.A. A Heuristic Home Electric Energy Management System Considering Renewable Energy Availability. *Energies* **2019**, *12*, 671. [[CrossRef](#)]
- Niknam, T.; Azizipanah-Abarghooee, R.; Roosta, A.; Amiri, B. A new multi-objective reserve constrained combined heat and power dynamic economic emission dispatch. *Energy* **2018**, *42*, 530–545. [[CrossRef](#)]
- Wang, R.; Sun, Q.; Hu, W.; Li, Y.; Ma, D.; Wang, P. SoC-Based Droop Coefficients Stability Region Analysis of the Battery for Stand-Alone Supply Systems With Constant Power Loads. *IEEE Trans. Power Electron.* **2021**, *36*, 7866–7879. [[CrossRef](#)]
- Xu, D.; Zhong, F.; Bai, Z.; Wu, Z.; Yang, X.; Gao, M. Real-time multi-energy demand response for high-renewable buildings. *Energy Build.* **2023**, *281*, 112764. [[CrossRef](#)]
- Sun, P.; Teng, Y.; Chen, Z. Robust coordinated optimization for multi-energy systems based on multiple thermal inertia numerical simulation and uncertainty analysis. *Appl. Energy* **2021**, *296*, 116982. [[CrossRef](#)]
- Cui, M.; Zhang, J.; Wu, H.; Hodge, B.-M. Wind-friendly flexible ramping product design in multi-timescale power system operations. *IEEE Trans. Sustain. Energy* **2017**, *8*, 1064–1075. [[CrossRef](#)]
- Teng, Y.; Sun, P.; Leng, O.; Chen, Z.; Zhou, G. Optimal Operation Strategy for Combined Heat and Power System Based on Solid Electric Thermal Storage Boiler and Thermal Inertia. *IEEE Access* **2019**, *7*, 180761–180770. [[CrossRef](#)]
- Nandakumar, N.; Annaswamy, A.M. Impact of increased renewables on natural gas markets in eastern united states. *J. Mod. Power Syst. Clean Energy* **2017**, *5*, 424–438. [[CrossRef](#)]

10. Nosair, H.; Bouffard, F. Flexibility envelopes for power system operational planning. *IEEE Trans. Sustain. Energy* **2015**, *6*, 800–809. [[CrossRef](#)]
11. Zhao, J.; Zheng, T.; Litvinov, E. A unified framework for defining and measuring flexibility in power system. *IEEE Trans. Power Syst.* **2015**, *31*, 339–347. [[CrossRef](#)]
12. Sun, P.; Yun, T.; Chen, Z. Multi-objective robust optimization of multi-energy microgrid with waste treatment. *Renew. Energy* **2021**, *178*, 1198–1210. [[CrossRef](#)]
13. Li, Y.; Gao, D.W.; Gao, W.; Zhang, H.; Zhou, J. Double-Mode Energy Management for Multi-Energy System via Distributed Dynamic Event-Triggered Newton-Raphson Algorithm. *IEEE Trans. Smart Grid* **2020**, *11*, 5339–5356. [[CrossRef](#)]
14. Zhao, J.; Zheng, T.; Litvinov, E. Variable resource dispatch through Do-Not-Exceed limit. *IEEE Trans. Power Syst.* **2015**, *30*, 820–828. [[CrossRef](#)]
15. Li, Y.; Zhang, H.; Liang, X.; Huang, B. Event-triggered based distributed cooperative energy management for multienergy systems. *IEEE Trans. Ind. Inf.* **2019**, *15*, 2008–2022. [[CrossRef](#)]
16. Rui, W.; Qiuye, S.; Dazhong, M.; Xuguang, H. Line Impedance Cooperative Stability Region Identification Method for Grid-Tied Inverters Under Weak Grids. *IEEE Trans. Smart Grid* **2020**, *11*, 2856–2866. [[CrossRef](#)]
17. Rui, W.; Qiuye, S.; Pinjia, Z.; Yonghao, G.; Dehao, Q.; Peng, W. Reduced-Order Transfer Function Model of the Droop-Controlled Inverter via Jordan Continued-Fraction Expansion. *IEEE Trans. Energy Convers.* **2020**, *35*, 1585–1595. [[CrossRef](#)]
18. Huang, W.J.; Zhang, N.; Yang, J.W.; Wang, Y.; Kang, C. Optimal Configuration Planning of Multi-Energy Systems Considering Distributed Renewable Energy. *IEEE Trans. Smart Grid* **2019**, *10*, 1452–1464. [[CrossRef](#)]
19. Fumo, N.; Mago, P.J.; Chamra, L.M. Emission operational strategy for combined cooling, heating, and power systems. *Appl. Energy* **2019**, *86*, 2344–2350. [[CrossRef](#)]
20. Zheng, J.; Zhou, Z.; Zhao, J.; Wang, J. Effects of the operation regulation modes of district heating system on an integrated heat and power dispatch system for wind power integration. *Appl. Energy* **2018**, *230*, 1126–1139. [[CrossRef](#)]
21. Cheng, X.; Lee, W.-J.; Sahni, M.; Cheng, Y.; Lee, L.K. Dynamic Equivalent Model Development to Improve the Operation Efficiency of Wind Farm. *IEEE Trans. Ind. Appl.* **2016**, *52*, 2759–2767. [[CrossRef](#)]
22. Teng, Y.; Sun, P.; Hui, Q.; Li, Y.; Chen, Z. A model of electro-thermal hybrid energy storage system for autonomous control capability enhancement of multi-energy microgrid. *CSEE J. Power Energy Syst.* **2019**, *5*, 489–497.
23. Li, J.F.; Xing, Y.; Huang, X.J. The Planning Method of the Multi-Energy Cloud Management Platform with Key Technologies and P2P Trade of Prosumers. *Processes* **2022**, *10*, 2272. [[CrossRef](#)]
24. Wang, R.; Ma, D.; Li, M.-J.; Sun, Q.; Zhang, H.; Wang, P. Accurate Current Sharing and Voltage Regulation in Hybrid Wind/Solar Systems: An Adaptive Dynamic Programming Approach. *IEEE Trans. Consum. Electron.* **2022**, *68*, 261–272. [[CrossRef](#)]
25. Sun, Z.; Shen, Y.; Chen, Z.; Teng, Y.; Qian, X. Interval Prediction Method for Wind Speed Based on ARQEA Optimized by Beta Distribution and SWLSTM. *Front. Energy Res.* **2022**, *10*, 927260. [[CrossRef](#)]
26. Jin, H.; Teng, Y.; Zhang, T.; Wang, Z.; Chen, Z. A deep neural network coordination model for electric heating and cooling loads based on IoT data. *CSEE J. Power Energy Syst.* **2020**, *6*, 22–30.
27. Teng, Y.; Hui, Q.; Chen, Z. Availability estimation of wind power forecasting and optimization of day-ahead unit commitment. *J. Mod. Power Syst. Cle.* **2019**, *7*, 1675–1683. [[CrossRef](#)]
28. Zheng, T.; Dai, Z.M.; Yao, J.H. Economic Dispatch of Multi-Energy System Considering Load Replaceability. *Processes* **2019**, *7*, 570. [[CrossRef](#)]
29. Wang, R.; Liu, H.; Li, M.-J.; Sun, Q.; Li, X.; Wang, P. Fast Charging Control Method for Electric Vehicle-to-Vehicle Energy Interaction Devices. *IEEE Trans. Transp. Electrif.* **2022**. *Early Access*. [[CrossRef](#)]
30. Li, Y.; Gao, D.W.; Gao, W.; Zhang, H.; Zhou, J. A Distributed Double-Newton Descent Algorithm for Cooperative Energy Management of Multiple Energy Bodies in Energy Internet. *IEEE Trans. Ind. Inf.* **2021**, *17*, 5993–6003. [[CrossRef](#)]
31. Hu, Z.; Liu, S.; Luo, W.; Wu, L. Intrusion-Detector-Dependent Distributed Economic Model Predictive Control for Load Frequency Regulation with PEVs Under Cyber Attacks. *Circuits and Systems I: Regular Papers. IEEE Trans.* **2021**, *68*, 3857–3868.
32. Hu, Z.; Liu, S.; Wu, L. Credibility-based distributed frequency estimation for plug-in electric vehicles participating in load frequency control. *Int. J. Electr. Power Energy Syst.* **2021**, *130*, 106997. [[CrossRef](#)]
33. Cheng, S.; Teng, Y.; Zuo, H.; Chen, Z. Power Balance Partition Control Based on Topology Characteristics of Multi-Source Energy Storage Nodes. *Front. Energy Res.* **2022**, *10*, 547. [[CrossRef](#)]
34. Tan, Z.; Guo, H.; Lin, H.; Tan, Q.; Yang, S.; Gejirifu, D.; Ju, L.; Song, X. Robust Scheduling Optimization Model for Multi-Energy Interdependent System Based on Energy Storage Technology and Ground-Source Heat Pump. *Processes* **2019**, *7*, 27. [[CrossRef](#)]
35. Ramos-Teodoro, J.; Gil, J.D.; Roca, L.; Rodriguez, F.; Berenguel, M. Optimal Water Management in Agro-Industrial Districts: An Energy Hub’s Case Study in the Southeast of Spain. *Processes* **2021**, *9*, 333. [[CrossRef](#)]

Disclaimer/Publisher’s Note: The statements, opinions and data contained in all publications are solely those of the individual author(s) and contributor(s) and not of MDPI and/or the editor(s). MDPI and/or the editor(s) disclaim responsibility for any injury to people or property resulting from any ideas, methods, instructions or products referred to in the content.